PERGAMON

Solid-State Electronics 43 (1999) 1725–1734

SOLID-STATE ELECTRONICS

Schottky and ohmic contacts to doped $Si_{1-x-y}Ge_xC_y$ layers

Jeff J. Peterson[a], Charles E. Hunt[a,*], McDonald Robinson[b]

[a]*Department of Electrical and Computer Engineering, University of California, Davis, CA 95616, USA*
[b]*Lawrence Semiconductor Research Laboratory, Inc, Tempe, AZ 85282, USA*

Received 29 November 1998; accepted 9 February 1999

Abstract

We report on titanium contacts to n-type and p-type $Si_{1-x-y}Ge_xC_y$ strained heteroepitaxial layers on (100)Si and material and electrical characterization of n-type and p-type platinum–silicide–germanide contacts to $Si_{1-x-y}Ge_xC_y$ strained heteroepitaxial layers on (100)Si. Ti contacts to n-type $Si_{1-x-y}Ge_xC_y$ show rectifying behavior at low doping levels but become ohmic as layers reach 10^{18} cm^{-3}. Ti contacts to p-type $Si_{1-x-y}Ge_xC_y$/Si are ohmic at doping levels as low as 10^{15} cm^{-3}. Contact resistances for Ti/$Si_{1-x-y}Ge_xC_y$ contacts had values ranging from 10^{-1} to 10^{-2} Ω cm^2.

X-ray diffraction (XRD) studies of rapid thermal anneal (RTA) silicidation of Pt on SiGeC indicate the reaction proceeds from elemental Pt to Pt_2(SiGeC) and ends in the Pt(SiGeC) phase, analogous to Pt/Si silicides. However, the Pt–silicide–germanide reaction with SiGeC requires higher temperatures than the counterpart Pt reaction with Si. Pt(SiGeC) contacts to n-type SiGeC layers show rectifying behavior with nonideality factors (n) of 1.02 to 1.05 and constant barrier heights of 0.67 eV independent of composition, indicating that Fermi level pinning relative to the SiGeC conduction band is occurring. For contact doping levels of 10^{18} cm^{-3} and above, Pt(SiGeC) contacts to n-type SiGeC layers are ohmic with constant contact resistance values of 10^{-2} Ω cm^2. Pt(SiGeC) contacts to p-type $Si_{1-x-y}Ge_xC_y$/Si were ohmic over the entire doping range studied, with resistances from the 1 Ω cm^2 range at intrinsic alloy doping levels, to the 10^{-2} Ω cm^2 range for doping levels of 10^{18} cm^{-3}.

Using Pt(SiGeC) ohmic contacts to p-type SiGeC, current–voltage measurements of $Si_{1-x-y}Ge_xC_y$ to (100)Si heterojunctions are also presented. Heterojunction barrier heights track the variation of the SiGeC energy bandgap to a factor of 0.84 × . The $Si_{1-x-y}Ge_xC_y$/Si heterojunction valence band discontinuity, ΔE_v, decreases 15 meV per %C incorporated into the strained alloy layer for $0 < y < 0.01$ and increases ΔE_v by 2.8 meV per %Ge for $0 < x < 0.11$.

1. Introduction

SiGe epitaxial layers on Si substrates (SiGe/Si) show promise to be a column IV alternative to III–V materials used in heterojunction and bandgap engineered devices. Psuedomorphically grown SiGe/Si layers are metastable, limiting both the epitaxial layer thickness and the thermal budget of subsequent fabrication steps through strain relaxation by the generation of dislocation defects at the SiGe/Si interface [1]. The addition of C to SiGe epitaxial layers extends the epitaxial layer stability by using the smaller C atoms to provide stress compensation in the SiGe layer, but has little effect to the epitaxial layer bandgap [2]. The resulting SiGeC/Si

* Corresponding author. Tel.: +1-530-752-1958.
E-mail address: hunt@ece.udavis.edu (C.E. Hunt)

0038-1101/99/$ - see front matter
PII: S0038-1101(99)00059-3

layer allows increased critical thickness over SiGe/Si layers of similar composition and shows greater endurance for subsequent thermal stresses. Relatively little, however, is known about SiGeC/Si material and electrical properties at this time.

The study of metal/SiGeC contacts and barrier heights is one area in which the understanding is still incomplete. Among the metal/SiGeC contact systems to have been studied are Al [3], Co [4], Ti [5] and W [6]. It is reported that Schottky contacts to p-type SiGeC show compositional dependence in the barrier height, while Schottky contacts to n-type SiGeC show no compositional dependence, an indication of Fermi level pinning [7]. Incorporation of C into the SiGe epitaxial layer has been shown in Refs. [3,5] to reduce epitaxial layer stress and relaxation during contact formation.

Some limited work has been done to understand the phase formation of metal/silicide–germanides in SiGeC. The phase formation of Co and Ti silicide–germanides on SiGeC epilayers has been shown to proceed through phase sequences identical with Si and SiGe, but at lower reaction rates [4,5]. Similar to silicide–germanide formation in SiGe, Ge has been shown to segregate from the silicide–germanide during formation, accumulating on the epilayer side of the interface. Both Donaton and Eyal report that C also segregates from the silicide–germanide to the silicide–germanide/epilayer interface during formation at temperatures in the 600°C range, perhaps causing reduced reaction rates in the silicide–germanide by impeding diffusion of reactants. For higher reaction temperatures on the order of 900°C, Donaton reports that C reincorporates back into the Co silicide–germanide during growth. Eyal et al. [5], showed the introduction of C into SiGe layers causes a marked decrease in strain relaxation in SiGe occurring during the Ti silicide–germanide reaction, indicating that SiGeC may prove to be a material which has advantages over SiGe for contacts using Ti. Further investigation of the Ti/SiGeC contact system is therefore an important step to developing Si and SiGeC compatible processes, since Ti/Si contacts play such a large part in today's Si integrated circuit process technologies.

Pt silicide–germanides are also investigated since Pt–silicide is widely used as a low-resistance contact to Si. Furthermore, Pt–silicide–germanide contacts to SiGe have application to IR detectors [13,14] and other devices. We report here the results of phase morphology and electrical characterizations of Pt silicide–germanide contacts to $Si_{1-x-y}Ge_xC_y$, $Si_{1-x}Ge_x$ and Si layers. Special attention is made to the characterization of Pt silicide–germanide contacts to p-type SiGeC as a method of studying SiGeC bandgap variation using the Pt material system. This compliments work done on the W material system by [6].

2. Experiment

Strained $Si_{1-x-y}Ge_xC_y$ epitaxial layers (x ranging from 0 to 0.29 and y ranging from 0 to 0.03) were grown on Si(100) wafers using dichlorosilane, germane and cyclopropane as precursors for atmospheric-pressure CVD at temperatures ranging from 625 to 675°C. SiGeC layers were doped n-type using phosphine or doped p-type using diborane, resulting in doping levels ranging from 10^{15} to 10^{18} cm^{-3} as measured by spreading resistance profiling (SRP). Using Rutherford backscattering spectrometry (RBS) measurements, these epilayers have been analyzed to determine alloy composition and crystallinity, which are used in comparing the material and device characteristics of the Pt silicide–germanide/SiGeC and Ti/SiGeC contacts.

Pt silicide–germanide contacts were prepared in the following manner. After an organic clean step, each sample was patterned for Pt liftoff using standard photolithographic techniques. Elemental Pt was then deposited to a thickness of 100 nm onto the SiGeC epilayer surface using electron-beam evaporation at 10^{-6} Torr. Liftoff and cleaning followed deposition. The samples were heated to silicide reaction temperatures using rapid thermal anneal (RTA) or standard furnace anneal steps. RTA was at 30 mTorr in N_2 ambient. Reaction time and temperature were set by using X-ray diffraction (XRD) to determine when silicide phases were completely reacted. Furnace reacted samples were annealed in atmospheric pressure N_2 for 30 min at temperatures ranging from 400 to 800°C. At this point, the Pt silicide–germanides were characterized using XRD, four point probe resistance measurement, and optical microscope inspection to determine the material qualities discussed in this work. Following formation of the Pt silicide–germanides, a 150 nm-thick oxide layer was deposited using low-temperature methods (electron beam SiO_2 evaporation or reactive RF Si sputtering) to insulate between the bondpad metallization and epilayers. After contact hole formation, liftoff photolithography and electron beam deposition of a 10 nm Ti diffusion barrier and a 500 nm Al layer completed the metallization. A contact anneal was done for 30 min at 400–425°C in a N_2 ambient. Finally, the oxide on the reverse of the wafer was removed. After photoresist removal, the Schottky diodes were measured for electrical characteristics. This process sequence results in 500- and 250-μm radius Pt silicide–germanide/SiGeC Schottky contacts (areas of 7.85×10^{-3} and 1.96×10^{-3} cm^2, respectively).

Ti contacts to SiGeC were also fabricated. After patterning a metal etch mask over the SiGeC/Si substrates, discrete SiGeC 'mesa' structures were formed by reactive ion etching exposed SiGeC areas away, leaving two different 'Greek cross' resistance test struc-

tures of 50- and 250-μm line widths, respectively and bar test structures of 100 μm line width. After etch mask removal and a standard RCA clean step, these structures were covered with an oxide layer at 425°C and patterned to define the contact holes. Following an additional clean step, 20 nm elemental Ti was evaporated using electron beam deposition at 10^{-6} Torr. Without disturbing vacuum, 500 nm of Al was deposited over the Ti layer for bondpad metallization. After metallization liftoff, a contact anneal was done for 30 min at 400–425°C in a N_2 ambient. The oxide on the wafer back side was also removed. The Ti/SiGeC contacts have areas of 1.6×10^{-3} cm^2.

Current–voltage measurements followed in a darkened ambient at 25°C on a temperature controlled wafer probe station using a HP4145 semiconductor parameter analyzer. Pt silicide–germanide/SiGeC Schottky diode I–V data was analyzed both graphically and using curve fitting methods. Both methods assume the diode operates under the TE (thermionic emission) Schottky diode model [8] and use the TE model to calculate J_s, ϕ_b and n. The series resistance, R_s, was also incorporated into the curve fitting, but is typically unnecessary when the data is fitted to low current values.

Another method used to determine the metal/SiGeC barrier height also assumes the TE model and is shown in the following equation [9,10]:

$$J(V_r) = A * T^2 \exp(-q\phi_b/kT). \quad (1)$$

Using Eq. (1), the reverse bias current at a fixed bias of −3 V was used to calculate the contact barrier height.

3. Results of silicide–germanide formation

Characterization of the phase transformation sequence of Pt silicide–germanides (these silicide–germanides will hereafter be referred to as $Pt_x(SiGeC)_y$) shows it to be similar to that of Pt on Si, although the formation temperature of $Pt_x(SiGeC)_y$ differs significantly from that of Pt_xSi. Completely reacted $Pt_x(SiGeC)_y$ is uniform in consistency and is similar in smoothness to the underlying SiGeC layers, having an average roughness of between 1 and 2 nm. Fig. 1 shows an example of a completely reacted silicide, which we will later show to be the Pt(SiGeC) phase. Fig. 2 shows an example of an incompletely-reacted silicide, which includes elemental Pt, $Pt_x(SiGeC)_y$ silicides and the final Pt(SiGeC) phase. This intermediate phase, rough and granular in appearance, had an average roughness in excess of 20 nm.

XRD and sheet resistance measurements were used to characterize the order of phase formation of the $Pt_x(SiGeC)_y$ silicides. Fig. 3 shows XRD spectra of the $Pt_x(SiGeC)_y$ phase transformation for a 600°C (Set Point) RTA. Fig. 3(a) shows that after 20 s of RTA the Pt film showed some evidence of $Pt_2(SiGeC)$ formation, but still shows a close match to the X-ray spectrum for Pt. Fig. 3(b) shows the spectrum after 80 s of 600°C RTA showing the reacted layer contains a

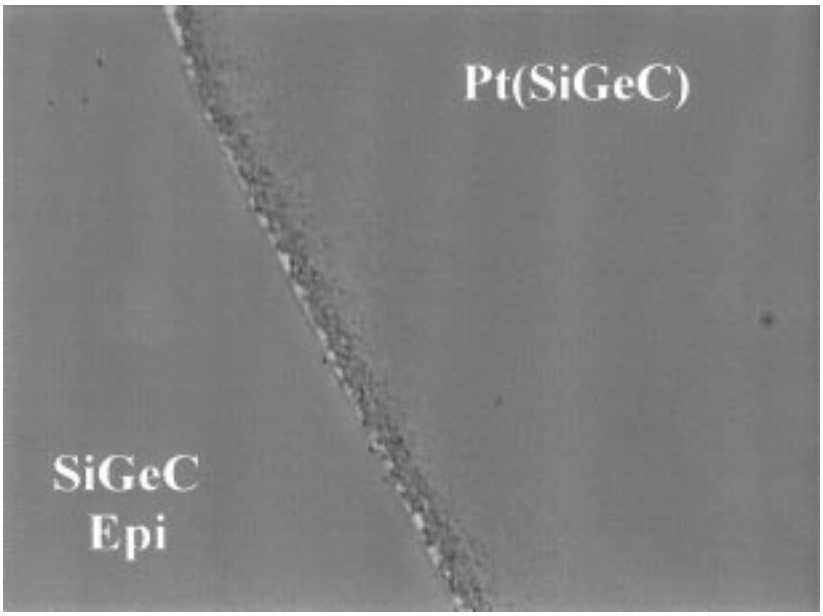

Fig. 1. Optical light-field micrograph showing the phase morphology of a completely reacted Pt(SiGeC) silicide (1000×).

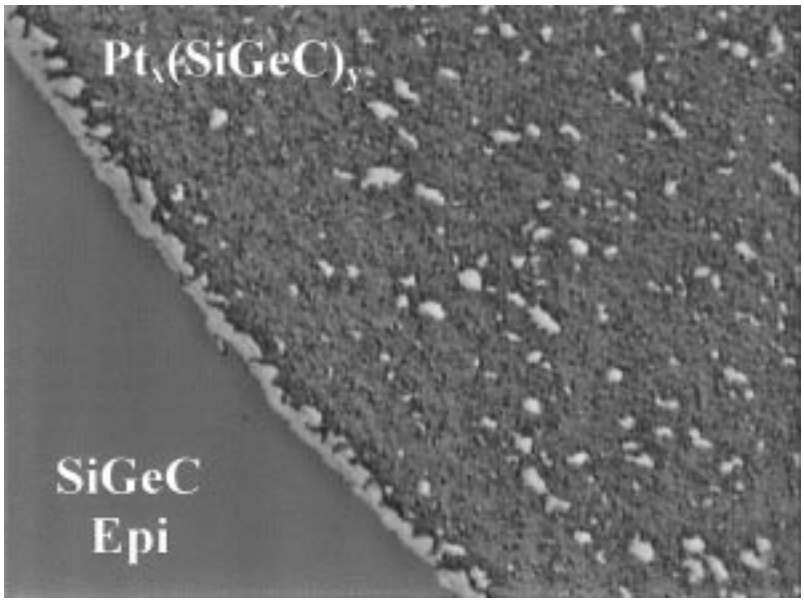

Fig. 2. Optical light-field micrograph showing the phase morphology of an incompletely reacted silicide composed of Pt, $Pt_x(SiGeC)_y$ and Pt(SiGeC) mixed phases (1000×).

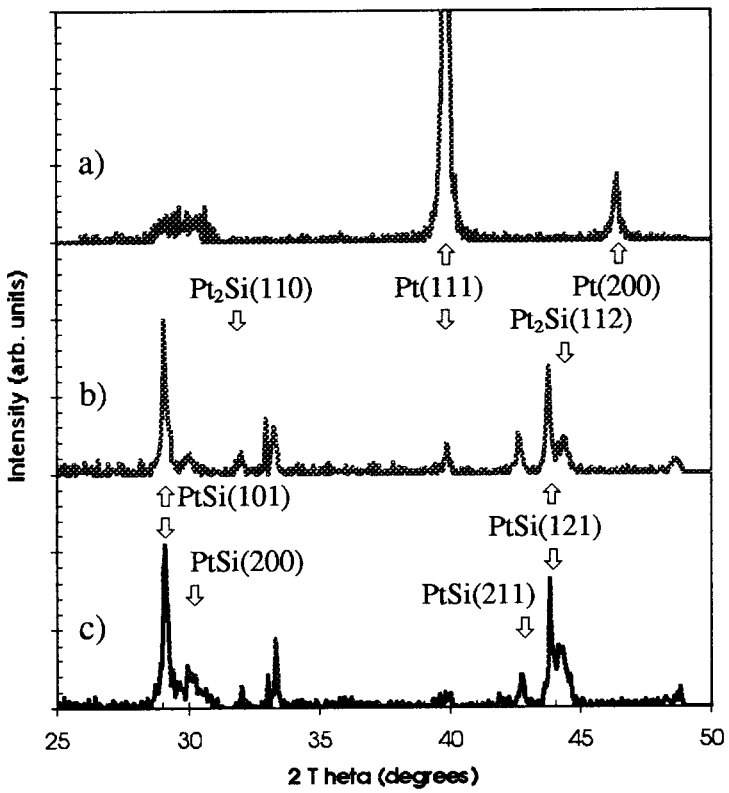

Fig. 3. XRD spectra of $Pt_x(SiGeC)_y$ phase with respect to RTA time. (a) XRD spectra after 20 s/600°C SP RTA showing elemental Pt, (b) XRD spectra after 80s/600°C SP RTA showing a mixture of Pt, Pt_2(SiGeC) and Pt(SiGeC), (c) XRD spectra after 160 s/600°C SP RTA showing completely reacted Pt(SiGeC).

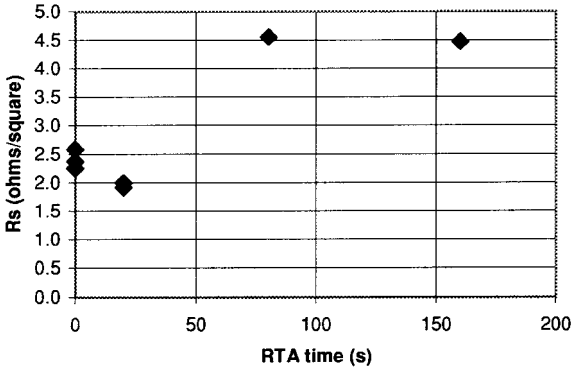

Fig. 4. R_s vs. 600°C SP RTA anneal time showing $Pt_x(SiGeC)_y$ phase formation beginning with elemental Pt, continuing to form low resistive $Pt_2(SiGeC)$, and completing with the formation of higher resistance Pt(SiGeC).

mixture of $Pt_2(SiGeC)$ and Pt(SiGeC) with a slight Pt signal still present. Fig. 3(c) shows the spectrum after 160 s of 600°C RTA; in this curve the silicide appears to be completely converted to the Pt(SiGeC) final phase. Additional annealing shows little change in the silicide, indicating the Pt(SiGeC) phase is the final phase. Pt/silicide–germanide in this report was annealed for at least 320 s of 600°C RTA to ensure complete phase transformation.

Sheet resistance (R_s) measurements were also used to characterize the $Pt_x(SiGeC)_y$ phase formation. For Pt/Si layers, Colgan showed R_s decreases as Pt_2Si formation takes place and increases again as the reaction completes at the PtSi phase [11]. Fig. 4 shows a graph of R_s vs. 600°C RTA anneal time. Similar to the results obtained by Colgan, the R_s lowers from the initial value of the elemental Pt film as the reaction begins to form $Pt_2(SiGeC)$. As the reaction proceeds, R_s rises, becoming constant as the silicide reaches the final Pt(SiGeC) phase. This is entirely consistant with the results of our XRD characterization and shows Pt silicide–germanide formation on $Si_{1-x-y}Ge_xC_y$ epitaxial layers follows a progression very similar to that for Pt silicide on Si, with the exception that the SiGeC composition also modifies the composition of the Pt silicide–germanide.

Rutherford backscattering spectrometry (RBS) measurements were also performed on these samples in order to analyze the Pt silicide–germanides for constituent segregation effects. RBS results show that Ge segregation from the Pt silicide–germanides does occur, with excess Ge accumulating at the silicide–germanide/SiGeC interface. These results are in agreement with those of both Donaton et al. [4] and Eyal et al. [5], who also report Ge segregation in Co and Ti contacts to SiGeC, respectively. We were unable to verify the existence of C segregation in Pt silicide–germanides using RBS.

Both RTA and standard furnace anneals of Pt/SiGeC required higher reaction temperatures than necessary for Pt/Si reactions. Standard furnace anneals of Pt/SiGeC showed initial Pt(SiGeC) phase formation at temperatures of 600°C, while, for Pt/Si, the silicide reaction begins at temperatures of about 300°C [11]. Donaton also reported higher temperatures in the formation of Co silicide–germanides on SiGeC [4]; this effect was attributed to Ge/C accumulation at the silicide–germanide/SiGeC interface (due to segregation effects) and to C precipitation at the higher temperatures.

4. Electrical characterization results

Several methods have been used to analyze these Schottky contacts for barrier height (ϕ_b), reverse-bias saturation current density (J_s), and the diode nonideality factor (n). Graphical analysis of the current–voltage (I–V) characteristic is used to find J_s, from which the contact barrier height is derived. The barrier height was also derived using Eq. (1), but this derivation must be done at low reverse-bias values to ensure the ϕ_b measurement is not affected by barrier height lowering at high reverse bias. Another method for analysis of the I–V data used mathematical curve-fitting to the Schottky diode thermionic emission model to extract the three parameters of interest. One additional method is used to find the diode nonideality factor, n: contact I–V data is plotted in $I/(1-e(-qV/kT))$ versus V form to obtain a flat curve from which to estimate n [12]; in order to account for series resistance effects, this method was used at low bias values.

4.1. Ti contacts to SiGeC

I–V analysis of Ti contacts to n-type SiGeC layers shows rectifying behavior at doping levels below 10^{17} cm^{-3}, but ohmic behavior as the doping reaches 10^{18} cm^{-3}. Fig. 5 shows results for Ti contacts to two SiGeC layers: a 10^{17} n-type doped $Si_{0.89}Ge_{0.1}C_{0.01}$ layer and a 10^{18} n-type doped $Si_{0.885}Ge_{0.1}C_{0.015}$ layer, respectively. While the lower doped contacts do not conduct until ~0.5 V, the 10^{18} cm^{-3} contacts are ohmic. This indicates n-type doping levels of 10^{18} cm^{-3} and above are sufficient to form ohmic Ti contacts to SiGeC, giving R_c in the 10^{-2} Ω cm^2 range; higher dopant concentrations could be used to obtain lower R_c values. This requirement is consistent with present-day Si-based processing.

Epilayer composition also affects the required contact doping level to achieve ohmic Ti contacts to n-type SiGeC. We expect that the increase in V_{bi}, which

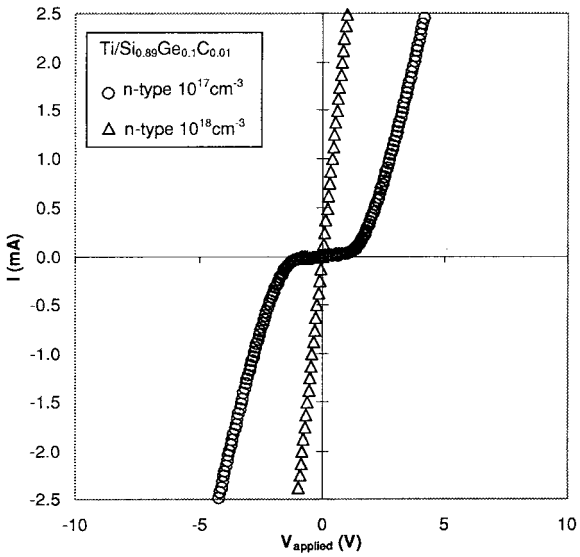

Fig. 5. I vs. $V_{applied}$ for $Ti/Si_{0.89}Ge_{0.1}C_{0.01}$ contact pairs. Open circle: 10^{17} cm^{-3} n-type epilayer doping. Open triangle: 10^{18} cm^{-3} n-type epilayer doping.

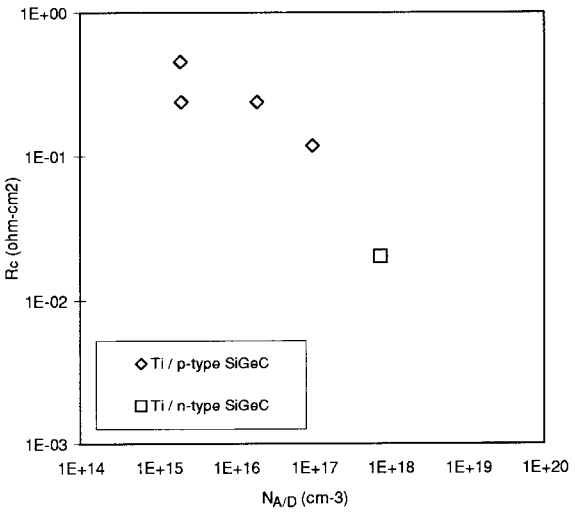

Fig. 6. Contact resistance (R_c) vs. contact layer doping for Ti contacts to n-type and p-type SiGeC. Open diamond: contacts to p-type. Open square: contacts to n-type.

accompanies a shrinking epilayer work function, would result in barrier lowering with further additions of Ge to the epilayer composition. We have investigated equivalently low-doped epi layers of various compositions and found rectifying behavior at low %Ge concentrations (i.e. a higher epilayer bandgap and work function) and ohmic contacts as the %Ge in the epilayers is increased (causing lower bandgap and shrinking work functions). For highly-doped contact layers, Ti contacts to both 10^{18} cm^{-3} n-type $Si_{0.715}Ge_{0.27}C_{0.015}$ epilayers and 10^{18} cm^{-3} n-type $Si_{0.885}Ge_{0.1}C_{0.015}$ epilayers proved to be ohmic.

Ti contacts to p-type $Si_{1-x-y}Ge_xC_y/Si$ were ohmic over the entire doping range we studied. Fig. 6 shows a plot of the R_c vs. epilayer doping for Ti contacts to both n-type and p-type SiGeC. From this plot, Ti contact resistances to p-type SiGeC are shown to be relatively high with values in the 0.1 Ω cm^2 range. Fig. 6 shows the contact resistance to drop $\sim$2/3 of a decade for each 10$\times$ increase in contact layer doping. From Fig. 6, it is also seen that Ti contact resistances to n-type SiGeC epilayers are smaller than those to p-type SiGeC epilayers for equivalent contact doping levels.

4.2. Pt(SiGeC) contacts to SiGeC

Pt–silicide–germanide contacts to n-type SiGeC layers were rectifying for contact dopant levels up to 5×10^{16} cm^{-3}. Fig. 7 plots log I vs. V for a Pt(SiGeC) contact to n-type SiGeC, demonstrating the Schottky-diode behavior for Pt–silicide–germanide contacts to n-type contacts with relatively low doping levels. Forward bias turn-on voltages were approximately 0.45 V with reverse bias breakdown voltages of roughly -8 V. Graphical methods showed the reverse bias current density, J_s, to be in the 10^{-5} A/cm^2 range. Nonideality factors (n) for Pt(SiGeC) contacts to n-type SiGeC ranged from 1.02 to 1.05. The graphical ϕ_b values (which we believe to be more accurate than the curve fitting ϕ_b values for these diodes) are independent of composition with an average value of 0.67 eV. This is in agreement with other results for metal/SiGeC contacts in the literature [6], which suggest Fermi level pinning relative to the conduction band in n-type SiGeC/Si removes the compositional dependence of ϕ_b for Schottky contacts to n-type SiGeC/Si layers. Our results are also consistent with Pt silicide Schottky barrier contacts to n-type SiGe which show Fermi pinning at values of 0.68 eV [15].

Pt(SiGeC) contacts to 10^{18} cm^{-3} n-type doped SiGeC were ohmic for silicide–germanide contacts. This indicates n-type doping levels of 10^{18} cm^{-3} and above are sufficient to form ohmic Pt contacts to SiGeC, giving R_c in the 10^{-2} Ω cm^2 range. Elemental Pt contacts to n-type doped SiGeC were also fabricated, but remained rectifying even at doping levels as high as 10^{18} cm^{-3}. This is reasonable since the Pt/SiGeC barrier heights are $\sim$60 mV higher than Pt silicide–germanide contacts to SiGeC if the trend seen by Pt and PtSi contacts to Si is followed [16]. Similar to Ti/SiGeC contacts, silicide–germanide contacts to n-type SiGeC should be doped 10^{18} cm^{-3} or higher for ohmic contacts. In addition, the Pt–silicide–germanide phase must be completely formed in order to achieve an ohmic contact.

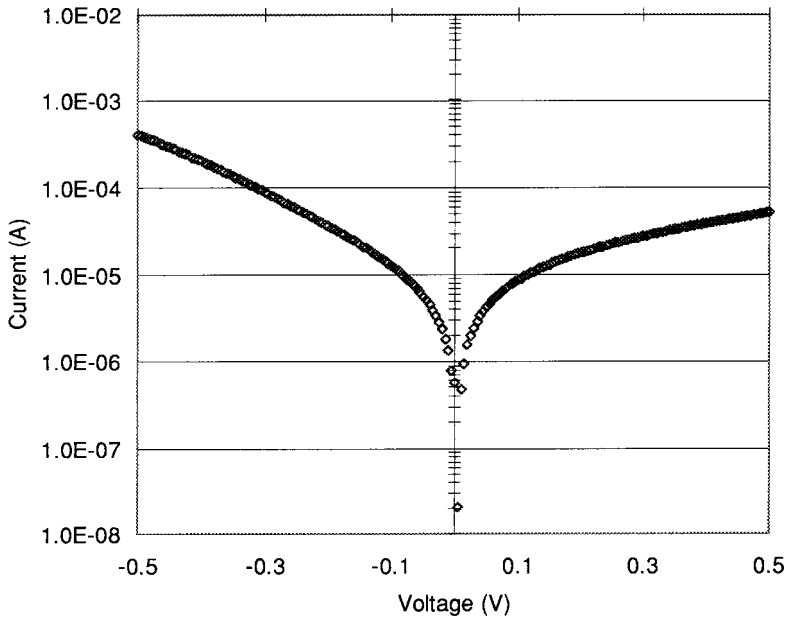

Fig. 7. Log I vs. V characteristic for Pt(SiGeC) contacts to N^+ SiGeC/Si.

We have also characterized Pt(SiGeC) contacts to p-type SiGeC and found them to be ohmic in the 10^{15}–10^{18} cm^{-3} doping range. Contacts with low doping levels had barrier heights starting from 0.48 eV, while higher contact doping levels resulted in measured barrier heights as low as 0.37 eV as calculated using Eq. (1). Fig. 8 displays a plot of R_c vs. contact doping for Pt(SiGeC) to p-type SiGeC contacts and for Pt(SiGeC) to n-type SiGeC contacts, respectively. As expected, increasing the contact doping decreases the contact re-

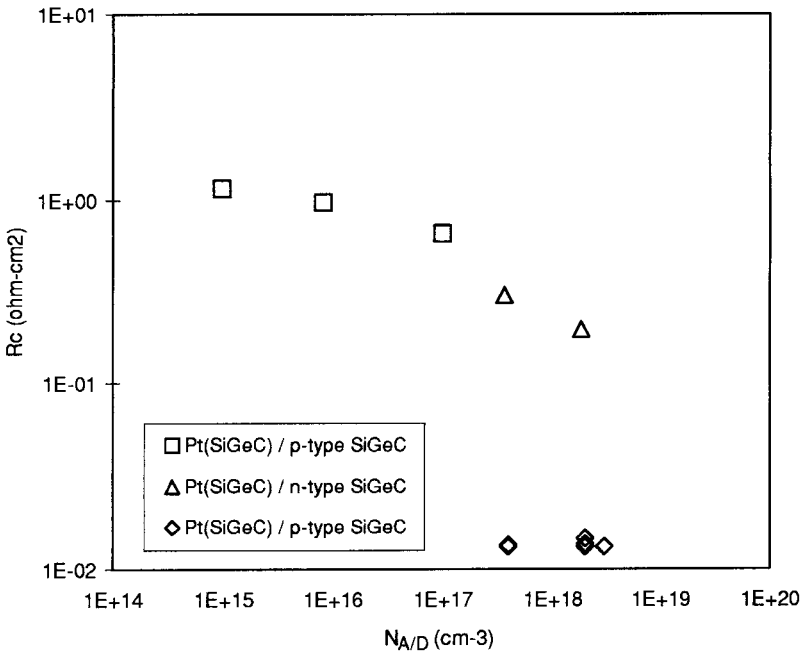

Fig. 8. Contact resistance (R_c) vs. contact layer doping for Pt(SiGeC) contacts to n-type and p-type SiGeC. Open square: contacts to p-type SiGeC. Open triangle: contacts to n-type SiGeC. Open diamond: contacts to p-type SiGeC.

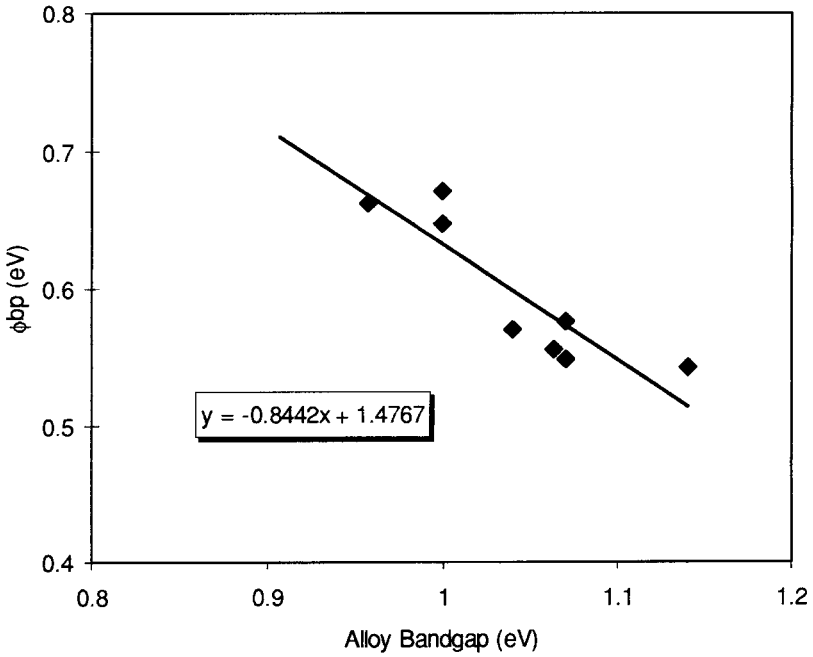

Fig. 9. P^+ $Si_{1-x-y}Ge_xC_y$ to (100) Si heterojunction measured barrier height vs. calculated epilayer bandgap for x ranging from 0 to 0.29 and y ranging from 0 to 0.03.

sistance. A 10× increase in contact doping level results in a 3–4× reduction in the contact resistance. Fig. 8 also shows that highly n-type doped Pt(SiGeC) ohmic contacts have a smaller contact resistance than comparably doped Pt(SiGeC) to p-type SiGeC contacts. As a comparison to Si, these data show that Pt(SiGeC) to SiGeC contacts will require substantially higher contact doping levels to achieve contact resistance values equivalent with those for PtSi contacts to Si.

4.3. Bandgap offset in p-type SiGeC

Finally, we describe the use of Pt silicide–germanide ohmic contacts to p-type SiGeC to characterize the energy bandgap discontinuity of $Si_{1-x-y}Ge_xC_y$ strained-layer heterojunctions on (100)Si. The goal is to measure the energy bandgap with varying composition and strain in the SiGeC alloy layer.

Using ohmic Pt(SiGeC) contacts to p-type SiGeC layers (described above), the I–V characteristics of the underlying heterojunctions were analyzed to determine the barrier height and other parameters of each junction. Heterojunction forward bias turn-on voltages (defined as the voltage required to reach 5 mA current) ranged from 0.8 V to 1.6 V depending on the alloy composition. Graphical measurement showed the reverse-thermal current density, J_s, to be in the 10^{-5} A/cm^2 range. Heterojunction nonideality factors (n) were found to vary from 1.10 to 2. If the substrate series resistance, which ranged from 35 Ω to over 100 Ω, is accounted for, n improves by ~5%.

From the reverse-bias current density values for eight $Si_{1-x-y}Ge_xC_y$/Si samples with $0 < x < 0.29$ and $0 < y < 0.03$, the barrier height for each heterojunction has been calculated. Fig. 9 plots the extracted p-type SiGeC to (100)Si heterojunction barrier height (ϕ_{bp}) versus the calculated energy bandgap for each SiGeC epilayer [17,18]. It is seen that ϕ_{bp} reduces at a rate roughly inverse to the bandgap increase. Using a least-squares linear fit to the data shows that the average correlation of ϕ_{bp} to the expected strained epilayer bandgap is $0.84 \times$. It is uncertain if the miscorrelation of ϕ_{bp} to E_g is due to experimental error or because the total bandgap value for each sample has been calculated rather than measured. (In the calculations we have made the simplification that any offset of the SiGeC and Si bandgaps will occur solely in the valence band, although this is not ascertained to be true).

We expect, for our device configuration, ϕ_{b_p} should correspond directly to ΔE_v, the valence band discontinuity. Therefore, we use the $Si_{1-x-y}Ge_xC_y$/Si heterojunction ϕ_{bp} values to estimate the effect C and Ge composition have on ΔE_v. Fig. 10 (a) shows the effect to ϕ_{bp} of adding C to strained epilayers of fixed Ge concentration ($x = 0.11$) for $y = 0$ and $y = 0.01$, respectively, as measured by RBS. These data indicate

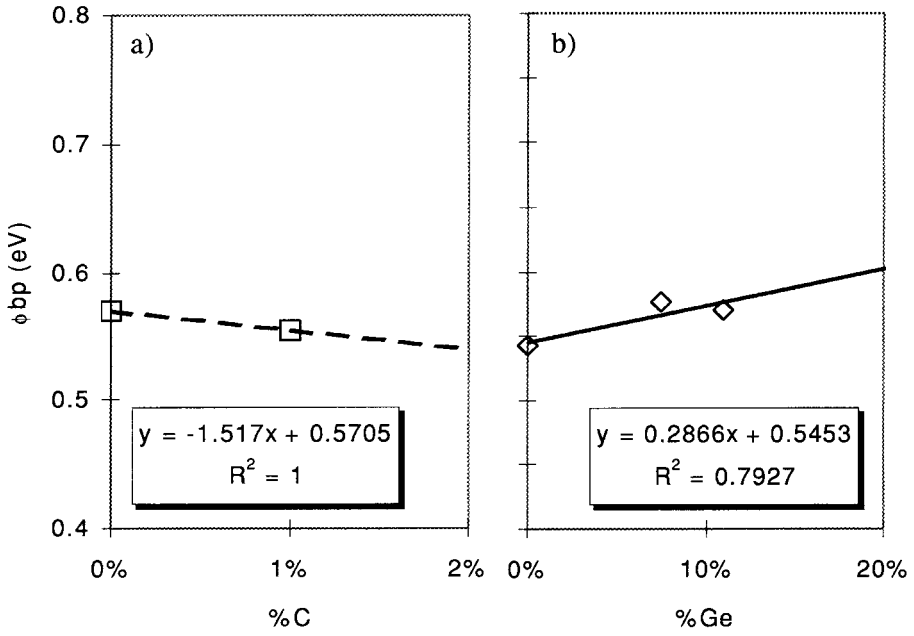

Fig. 10. ϕ_{bp} vs. strained P^+ $Si_{1-x-y}Ge_xC_y$ composition. (a) ϕ_{bp} vs. %C for $0 < x < 0.11$ and for $0 < y < 0.01$; curve fit shows ϕ_{bp} is reduced by 15 meV per %C as a result of C incorporation. (b) ϕ_{bp} vs. %Ge for $y = 0$ and for $x = 0$ to $x = 0.11$; curve fit shows ϕ_{bp} increases 2.8 meV per %Ge incorporation.

ΔE_v decreases by 15 meV per %C. These results show less influence due to the inclusion of C when compared with the data by Chang et al. [19] which showed, as measured by C–V techniques, a ΔE_v reduction of 20–26 meV per %C. The discrepancy can be partially attributed to our use of total C concentration (as measured by RBS) while Chang et al. quotes results for substitutional C only. Fig. 10 (b) shows the effect on ΔE_v of adding Ge to a $Si_{1-x-y}Ge_xC_y$ strained epilayer on (100)Si for $y = 0$ and $0 < x < 0.11$. In this case, our data indicates ΔE_v to increase 2.8 meV per %Ge, which is less than the range of 7.5–8.4 meV per %Ge which some others have published [20,21]. Again, our data reflect the total Ge inclusion as measured by RBS.

5. Conclusions

We have electrically characterized titanium and platinum–silicide–germanide contacts to n-type and p-type $Si_{1-x-y}Ge_xC_y$ strained epilayers on Si(100). Ti contacts to n-type SiGeC show rectifying behavior at low doping values, but become ohmic as doping in the layers reaches 10^{18} cm^{-3}, with contact resistances of 10^{-2} Ω cm^2. Ti contacts to p-type SiGeC are ohmic at doping levels as low as 10^{15} cm^{-3}, becoming less resistive as contact doping levels are increased.

Electrical characterization of low-doped Pt(SiGeC) contacts to n-type SiGeC shows rectifying behavior with nonideality factors of $1.02 < n < 1.05$ and constant barrier heights of 0.67 eV independent of composition, indicating Fermi-level pinning relative to the SiGeC conduction band is occurring. Pt(SiGeC) contacts to n-type $Si_{1-x-y}Ge_xC_y$ are ohmic for doping levels of 10^{18} cm^{-3} and above, with contact resistance values of 10^{-2} Ω cm^2 for doping levels of 10^{18} cm^{-3}. Pt(SiGeC) contacts to p-type $Si_{1-x-y}Ge_xC_y$/Si were ohmic over the entire doping range studied, with contact resistances ranging from 1 Ω cm^2 for intrinsic alloys to the 10^{-2} Ω cm^2 for doping at 10^{18} cm^{-3}.

We also report the material characterization of n-type and p-type Pt silicide–germanide contacts to $Si_{1-x-y}Ge_xC_y$ epitaxial layers. We find the silicidation reaction of SiGeC to proceed from elemental Pt to Pt_2(SiGeC) and to terminate with the Pt(SiGeC) phase. The Pt silicide–germanide reaction with SiGeC is shown to require higher temperatures than the analogous Pt reaction with Si.

I–V measurements of the $Si_{1-x-y}Ge_xC_y$ to (100)Si heterojunction indicate the heterojunction barrier height is inversely proportional to the SiGeC bandgap by a factor of $0.84\times$. The $Si_{1-x-y}Ge_xC_y$ to (100)Si heterojunction valence band discontinuity, ΔE_v, decreases 15 meV per %C incorporated into the

strained alloy layer and increases 2.8 meV per %Ge incorporated.

Acknowledgements

This project was supported by Lawrence Semiconductor Research Laboratories, Inc, UC MICRO, and ONR contracts #N00014-93-C-0114 and #N00014-96-C-0219. Devices were fabricated in the UC Davis Microfabrication Facility.

References

[1] Bean JC. IEEE Proc 1992;80(4):571–87.
[2] Powell AR, Eberl K, Ek BA, Iyer SS. J Crystal Growth 1993;127:425–9.
[3] Mi J, Gupta A, Yang CY, Zhu J, Yu PKL, Warren P, Dutoit M. Appl Phys Lett 1996;69(24):3743–5.
[4] Donaton RA, Maex K, Vantomme A, Langouche G, Morciaux Y, Amour A St, Sturm JC. Appl Phys Lett 1997;70(10):1266–8.
[5] Eyal A, Brener R, Beserman R, Eizenberg M, Atzmon Z, Smith DJ, Mayer JW. Appl Phys Lett 1996;69(1):64–6.
[6] Mamor M, Guedj C, Boucaud P, Meyer F, Bouchier D, Bodnar S, Regolini JL. Strained layer epitaxy: materials, processing, and device applications. In: Fitzgerald E, Hoyt J, Cheng K, Bean J, editors. Mater Res Soc Proc, vol. 379, Pittsburg, PA, 1995. p. 137–41.
[7] Meyer F, Mamor M, Aubry-Fortuna V, Warren P, Bodnar S, Dutartre D, Regolini JL. J Elec Mater 1996;25(11):1748–53.
[8] Shur M. In: Physics of semiconductor devices. Englewood Cliffs, NJ: Prentice Hall, 1990. p. 205.
[9] Rhoderick EH, Williams RH. In: Metal–semiconductor contacts. New York: Oxford University Press, 1988. p. 124.
[10] Sze SM. In: Physics of semiconductor devices. New York: John Wiley & Sons, Inc, 1981. p. 258.
[11] Colgan EG. J Mater Res 1995;10(8):1953–7.
[12] Schroder DK. In: Semiconductor material and device characterization. New York: John Wiley & Sons, Inc, 1990. p. 187.
[13] Kanaya H, Hasegawa F, Yamaka E, Moriyama T, Nakajima M. Jpn J Appl Phys 1989;28(4):L544–L546.
[14] Xiao X, Sturm JC, Parihar SR, Lyon SA, Meyerhofer D, Palfrey S, Shallcross FV. Electron Dev Lett 1993;14(4):199–201.
[15] Liou HK, Wu X, Gennser U, Kesan VP, Iyer SS, Tu KN, Yang ES. Appl Phys Lett 1992;60(5):577–9.
[16] Sze SM. In: Physics of semiconductor devices. New York: John Wiley & Sons, Inc, 1981. p. 291–2.
[17] S.C. Jain, Germanium–silicon strained layers and heterostructures, Academic Press, San Diego, 1994, p. 115.
[18] Stein BL, Yu ET, Croke ET, Hunter AT, Laursen T, Mayer JW, Ahn CC. J Vac Sci Technol B 1998;16(3):1639–43.
[19] Chang CL, Amour A, St Sturm JC. Appl Phys Lett 1997;70(12):1557–9.
[20] Colombo L, Resta R, Baroni S. Phys Rev B 1991;44:5572–9.
[21] Van de Walle CG, Martin RM. Phys Rev B 1986;34(8):5621–34.